Size-Dependent Suppression of Molecular Diffusivity in Expandable

Hydrogels: A Single-Molecule Study

Ha H. Park, Alexander A. Choi, and Ke Xu*

Department of Chemistry, University of California, Berkeley, Berkeley, CA 94720

ABSTRACT

By repurposing the recently popularized expansion microscopy to control the meshwork size of hydrogels, we examine the size-dependent suppression of molecular diffusivity in the resultant tuned hydrogel nanomatrices over a wide range of polymer fractions of ~0.14–7 wt%. With our recently developed single-molecule displacement/diffusivity mapping (SMdM) microscopy methods, we thus show that with a fixed meshwork size, larger molecules exhibit more impeded diffusion, and that for the same molecule, diffusion is progressively more suppressed as the meshwork size is reduced, and this effect is more prominent for the larger molecules. Moreover, we show that the meshwork-induced obstruction of diffusion is uncoupled from the suppression of diffusion due to increased solution viscosities. Thus, the two mechanisms, respectively being diffuser-size dependent and independent, may separately scale down molecular diffusivity to produce the final diffusion slowdown in complex systems like the cell.

KEYWORDS

Molecular diffusion, single-molecule spectroscopy, expandable hydrogel, size-dependent diffusion scaling, expansion microscopy.

1

TEXT

Introduction

Molecular diffusion underlies vital physical and chemical processes that govern the dynamic behaviors of non-equilibrium systems, including the living cell. However, it remains unresolved how and why the intracellular molecular diffusivity scales with the diffuser size. Whereas current models often assume that for molecules $<\sim$ 30 kDa, the intracellular diffusion coefficients D are \sim 25% of that *in vitro* ($D_{\rm cyto}/D_{\rm water} \sim$ 0.25), and that this ratio drops substantially to $<\sim$ 0.05 for molecules $>\sim$ 50 kDa, 1,5,8 we and collaborators have recently shown that in the mammalian cell, the diffusion of small ($<\sim$ 1 kDa) molecules is only modestly suppressed to $D_{\rm cyto}/D_{\rm water} \sim$ 0.7, 11 and that in the bacterial cytoplasm, $D_{\rm cyto}/D_{\rm water}$ drops slowly over the 20-300 kDa range. 10

Suppressed intracellular diffusion beyond that is expected from the modestly (20-40%) higher viscosity of the cytosol over water¹² is often attributed to obstruction from the nanoscale architectures in the cell. An earlier study has shown that nanomatrices/meshworks formed by crosslinked actin filaments partly recapitulate the diffuser size-dependent slowdown of diffusion, so that at 8 mg/mL (~0.8 wt%) actin, substantial suppressions of D are observed for large DNA molecules.⁷ In contrast, no diffuser size-dependent diffusion slowdown is observed with alternative crowding agents such as cytosol or Ficoll-70 polymer solutions, thus emphasizing the importance of crosslinked meshworks, i.e., hydrogels, in the size-dependent obstruction of the diffusion of large molecules. Apart from providing a valuable platform to understand obstructed diffusion, molecular diffusion in hydrogels also plays vital roles in diverse biomedical, chemical, and materials applications ranging from drug delivery to separation science. 13-16 Recent years have seen increased interest in examining the diffusion and dynamics of biomolecules and particles in synthetic hydrogels with modern microscopy tools. 14,17-19 However, as each study only tests a few polymer conditions defined by the starting monomer concentrations, they do not provide a complete picture of how the evolution of the meshwork size gives rise to transitions between unimpeded and impeded diffusions. Varying the starting monomer concentrations may further affect the polymerization kinetics and lead to altered microscopic structures beyond simple rescaling of the meshwork size.²⁰ Thus, it remains a challenge to elucidate how the meshwork size itself controls obstructed diffusion.

In this work, we achieve continuous fine-tuning of the hydrogel nanomatrix meshwork size by borrowing the recent success of expandable hydrogels with high-resolution microscopy, ^{21,22} including single-molecule and super-resolution microscopy applications.²³⁻²⁶ By starting with the same monomer concentrations for polymerization and then differently expanding the resultant hydrogel, this approach leaves the geometric expansion of meshwork size as the only variable. Integrating our recent development of single-molecule displacement/diffusivity mapping (SMdM), 11,27-29 which measures D with high fidelity via stroboscopic-illumination-enabled widefield detection of diffusing single molecules, 30,31 we quantify diffusion-hindering effects in this controllably tuned system. We thus show that under the same hydrogel expansion condition and hence a constant meshwork size, increasingly impeded diffusion occurs for the larger molecules. By fine-tuning the expansion ratio to achieve a wide range of polymer fractions of $\sim 0.14-7$ wt%, we then show that for the same molecule, diffusion is progressively more suppressed with reducing meshwork sizes, and that this effect is more prominent for the larger molecules. Moreover, we show that the meshwork-induced obstruction of diffusion is uncoupled from diffusion suppressions due to increased solution viscosity, so the two mechanisms may separately scale down D to produce the final diffusion slowdown.

Materials and Methods

Preparation of fluorescence dye-labeled proteins. Ribonuclease (RNase) A (Sigma, R5500) and bovine serum albumin (BSA, Sigma, A3059) were labeled with Cy3B or Alexa Fluor 647 (AF647) via NHS (*N*-hydroxysuccinimide) ester conjugation. Cy3B-NHS (Cytiva, PA63101) or AF647-NHS (ThermoFisher, A37573) were mixed with protein in 0.1 M NaHCO₃ at a 10:1 dye-to-protein ratio, incubated at room temperature for 1.5 hr, are then purified with 3k and 10k MWCO centrifugal filters, respectively (Millipore, UFC500396 and UFC501096). The resultant dye-to-protein ratios were 0.5-1.5, as determined with a NanoDrop 2000c spectrometer (ThermoFisher). Dye-labeled RNase A was further treated with sulfo-NHS-acetate (ThermoFisher, 26777) to cap the excessive lysines. For immunoglobulin G (IgG), a commercial AF647-labeled goat anti-mouse secondary antibody (ThermoFisher, A21236) was used.

Preparation of expandable hydrogel. Sodium acrylate (Sigma, 48220), acrylamide (Sigma, A9099), *N*,*N*'-methylenebisacrylamide (MBAA, Sigma, M7279), *N*,*N*,*N*',*N*'-tetramethyl ethylenediamine (TEMED, Sigma, T7024) and ammonium persulfate (APS, Sigma, A3678) were prepared as stock solutions of 0.38, 0.5, 0.02, 0.1, and 0.1 g/mL in water, respectively. Monomer mixture solutions were prepared from the stock solutions to 1.25 M total concentrations with varied sodium acrylate and acrylamide mole fractions and a fixed 0.8% mole fraction of MBAA. To initiate polymerization, TEMED and APS were added, both to 0.2% wt. in the final mixture, and the mixture was quickly injected into a gel-formation

chamber (Figure S1) adopted and modified from standardized expansion-microscopy protocols. ^{32,33} The assembly was placed in a 37 °C humidified incubator for 30 min. The chamber was dissembled, and the lengths of the four edges of the resultant hydrogel were measured. Each hydrogel was then expanded in a solution of a fixed ionic strength for 10 min, followed by a racial-quenching solution of the same ionic strength but with the addition of 1 mM of 4-hydroxy-TEMPO (Sigma, 176141) for 30 min, and then the same expanding solution without 4-hydroxy-TEMPO for 10 min. Ionic strengths lower or higher than that of phosphate-buffered saline (PBS; 14190144, Gibco) (160 mM) were prepared by diluting PBS with Milli-Q water or by adding NaCl to PBS, respectively. To infuse dyes and dye-labeled proteins, the hydrogel was immersed in the same expanding solution with the addition of 150-300 pM of the fluorescent probe for 10-20 min. The dimensions of the hydrogel were remeasured, and the averaged length ratio over that before the expansion was taken as the expansion factor. Excess solution was removed, and the hydrogel was transferred onto a BSA-passivated 25-mm diameter #1.5 coverslip, and mounted into the coverslip holder (ThermoFisher, A7816). Coverslip passivation was done through the sequential sonication in acetone and Milli-Q water for 5 min each, treating with 10 mg/mL BSA in PBS for 30 min, rinsing with Milli-Q water, and drying with N₂ gas.

Optical setup. SMdM was performed on a Nikon Ti-E inverted fluorescence microscope, as described previously.²⁷⁻²⁹ A 561-nm laser (OBIS 561 LS, Coherent, 165 mW) and a 642-nm laser (Stradus 642, Vortran, 110 mW) were focused at the back focal plane of an oil-immersion objective lens (Nikon CFI Plan Apochromat λ 100×, numerical aperture 1.45). A translation stage shifted the laser beams toward the edge of the objective lens to reach the sample at an incidence angle slightly below the critical angle of the coverslip-hydrogel interface, thus illuminating a few micrometers into the hydrogel. Single-molecule images were collected 1.5-2 μm away from the coverslip surface. Fluorescence emission under 561 nm excitation was filtered by long-pass (ET575lp, Chroma) and band-pass (ET605/70m, Chroma) filters. Fluorescence emission under 642 nm excitation was filtered by long-pass (ET655lp, Chroma) and band-pass (ET705/100m, Chroma) filters. Wide-field single-molecule images were collected at 110 frames per second for 5,000-8,000 frames with an EM-CCD camera (iXon Ultra 897, Andor). For SMdM pulse control, the excitation lasers were modulated by a multifunctional input/output board (PCI-6733, National Instruments), which read the EMCCD camera exposure output signal to enable pulse-frame synchronization. Tandem laser pulse sequences were applied at fixed center-to-center separations Δt of 400 or 600 μs, with corresponding pulse durations set at 200 and 400 μs, respectively.

SM*d***M** data analysis. SM*d*M data were analyzed as described previously.²⁷ Briefly, single molecules were super-localized in each recorded frame, and their two-dimensional displacements between paired frames were calculated. The accumulated displacements were fitted through maximum likelihood estimation (MLE) to a probability model based on two-dimensional random walk:²⁷

$$P(r) = \frac{2r}{a} \exp(-\frac{r^2}{a}) + br \qquad \text{(eqn. 1)}$$

where r is the single-molecule displacement in the fixed time interval Δt (400 or 600 μ s as described above), $a = 4D\Delta t$, and b is a background term accounting for mismatched molecules that randomly diffuse into the

field of view during Δt , as discussed previously.²⁷ The mle function of MATLAB returned 95% confidence intervals for D.

Results and Discussion

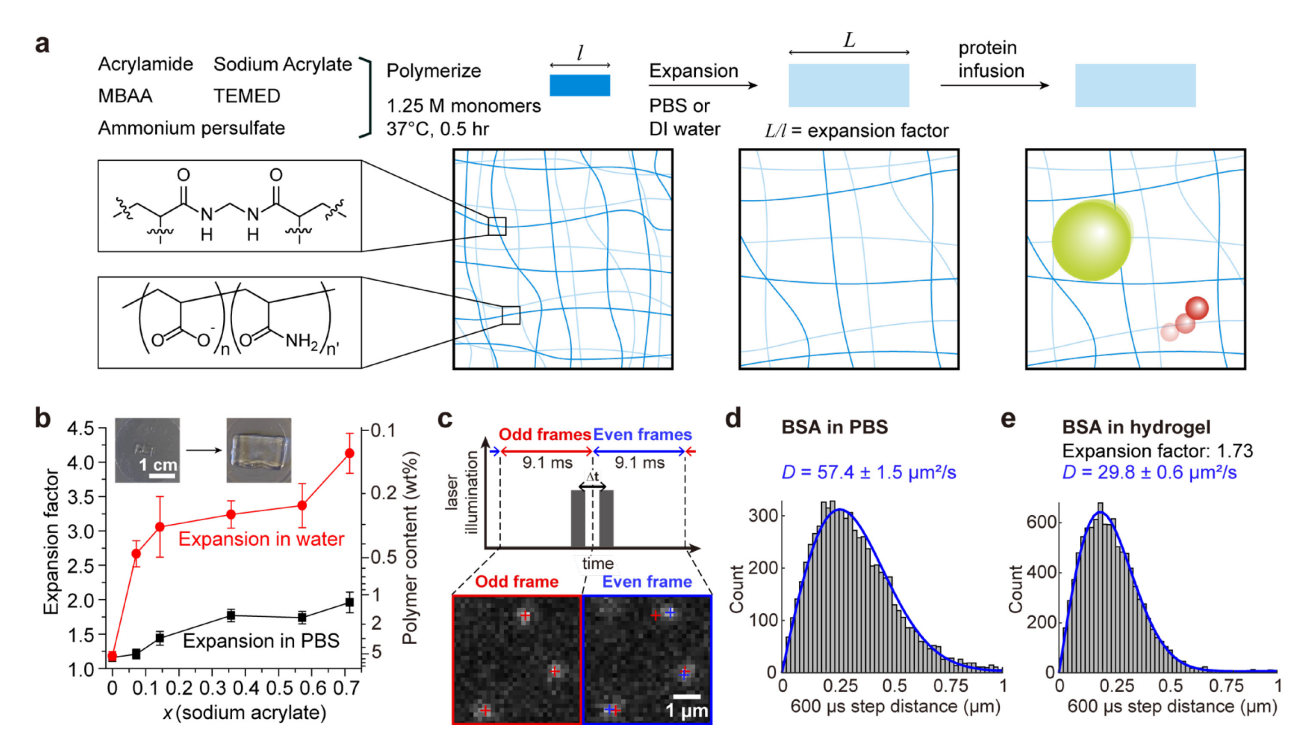


Figure 1. Controlled expansion of hydrogels for the SMdM quantification of molecular diffusion in tuned nanomatrices. (a) Schematic: N,N'-methylenebisacrylamide (MBAA)-crosslinked copolymerization of acrylamide and sodium acrylate generates a hydrogel network that expands isotropically in aqueous solutions. The degree of expansion is controlled by the sodium acrylate fraction and the ionic strength of the solution, hence tunable nanomatrix pore sizes for examining size-dependent molecular diffusion. (b) Measured expansion factor (left y-axis), as defined by the length ratio of the hydrogel after and before the expansion, and corresponding polymer wt% content of the expanded hydrogel (right y-axis), for hydrogels polymerized from different mole fractions of sodium acrylate and then expanded in the PBS (black) or water (red). Error bars: standard deviations between different runs. Inset: photos of a sample before and after 2.98x expansion in water. (c) SMdM: paired stroboscopic illumination pulses across tandem camera frames enable the detection of single-molecule displacements over a short time window, e.g., $\Delta t = 600 \,\mu s$ for the example images shown for Cy3B-labeled BSA diffusing in an expanded hydrogel. The paired excitation scheme is repeated ~6,000 times to establish statistics. (d,e) Example distributions of 600-µs single-molecule displacements for Cy3B-labeled BSA freely diffusing in PBS (d) vs. in a hydrogel expanded by 1.72x in PBS (e). Blue curves: Maximum likelihood estimation (MLE) with our diffusion model, yielding $D = 57.4 \pm 1.5$ and $29.8 \pm 0.6 \,\mu\text{m}^2/\text{s}$ (95% confidence intervals), respectively.

Expansion microscopy^{21,22} starts by embedding a (biological) sample in a swellable ionic hydrogel^{34,35} of crosslinked poly(acrylamide-*co*-sodium acrylate). Upon hydration, the hydrogel expands isotropically owing to the repulsing charges on the acrylate residues on the polymer chain. Whereas most expansion-microscopy applications use the maximal expansion (~4.5× in each dimension; ~100× in volume) to enlarge structural details, we reason that this system may be repurposed to generate continuously tunable matrix pore sizes and polymer fractions in the final hydrogel, ideal for elucidating the size-dependent diffusion properties of macro(bio)molecules (Figure 1a and Figure S1).

Thus, starting with a fixed total amount (1.25 M; 8.9 wt%) of acrylamide and sodium acrylate monomers and the same amount (0.8 mol% of monomers) of the crosslinker *N*,*N*'-methylenebisacrylamide (MBAA), we varied the sodium acrylate fraction to generate hydrogels of different expansibilities. Expansion factors, as defined by the length ratios of the hydrogel after and before the expansion (Figure S1), were thus attained in the range of 1.1–4 (Figure 1b; left y-axis), hence ~7–0.14 wt% polymer fractions in the expanded gel (Figure 1b; right y-axis). Higher expansion factors were obtained with increased sodium acrylate fractions, and the expansion factor could be further fine-tuned in a reversible fashion by adjusting the solution ionic strength (Figure S2).

To characterize molecular diffusion in the hydrogels, we integrated our recently developed SMdM. $^{27-29}$ In SMdM, fast-diffusing single molecules are imaged in the wide field by reducing motion blur via stroboscopic excitation. 30,31 The stroboscopic pulses are applied in tandem across odd-even camera frames at short time separations of $\Delta t < 1$ ms (Figure 1c), thus allowing for the determination of single-molecule displacements in the Δt time window. By continuously running this tandem stroboscopic excitation scheme at 110 frames per second, we thus accumulated the transient displacements of $>10^4$ single molecules (Figure 1de) across the camera frame in ~ 1 min. Fitting the resultant displacement distributions to a random-walk model (Methods) yielded diffusion coefficient D with $<\pm 3\%$ brackets at 95% confidence intervals (Figure 1de). We thus found, for example, the diffusion coefficient of the 67 kDa protein bovine serum albumin (BSA) inside a hydrogel expanded in the phosphate-buffered saline (PBS) by a factor of $1.73\times (5.2\times volume\ expansion;\ 1.7\ wt\%$ final polymer content) was 52% of that measured in PBS itself (Figure 1de).

To examine how the polymer meshwork may differently suppress the diffusion of molecules of varied sizes, we quantified the diffusion coefficient D of the 0.6 kDa free dye Cy3B and dye-labeled proteins, the 14 kDa ribonuclease A (RNase A), the 67 kDa BSA, and the 150 kDa immunoglobulin G (IgG), in PBS and in hydrogels of two contrasting expansion factors. Here we chose four highly water-soluble targets that substantially differ from each other in size, so that the size effect may stand out over other potential factors as molecular shape and hydrophobicity. For diffusion in PBS, SMdM yielded D values in the range of 40–350 μ m 2 /s that dropped monotonically with the molecular weight M (Figure S3), comparable to our previous results 29 affirming the $D\sim M^{-1/3}$ model of Young-Carroad-Bell, 36 and we obtained similar D values with Δt = 400 and 600 μ s (Figure S3).

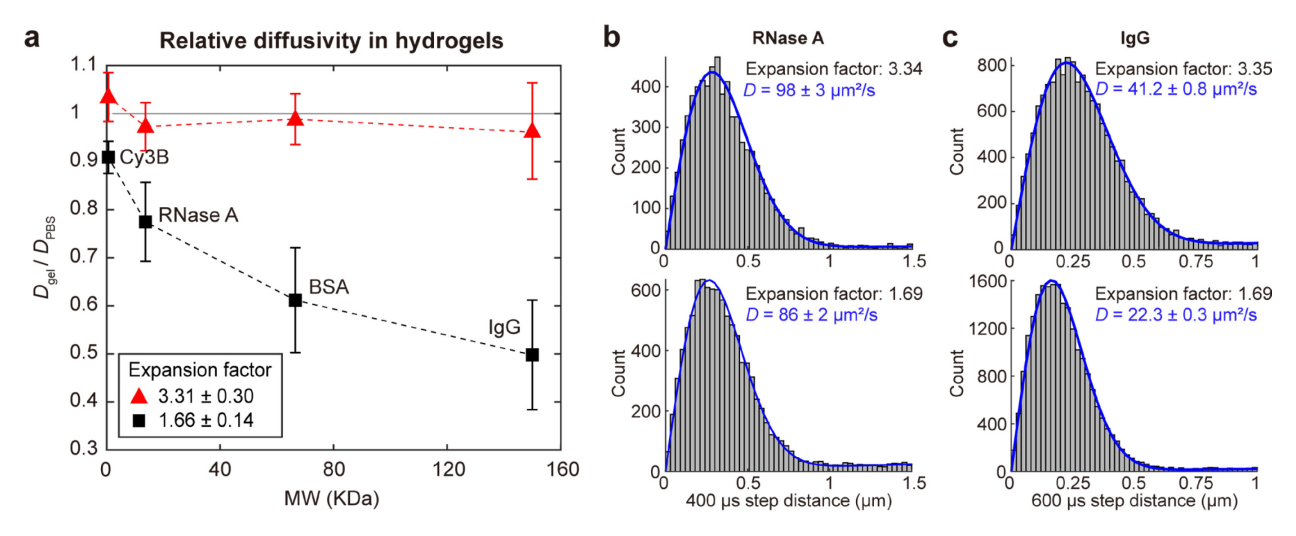


Figure 2. Molecular size-dependent suppression of diffusivity in hydrogels differently expanded in PBS and in water. (a) SMdM-determined in-gel diffusion coefficient D relative to that in the PBS buffer for the 0.6 kDa free dye Cy3B and dye-labeled proteins, the 14 kDa ribonuclease A (RNase A), 67 kDa bovine serum albumin (BSA), and 150 kDa immunoglobulin G (IgG), in hydrogels expanded by 1.66 \pm 0.14 in PBS (black) vs. by 3.31 \pm 0.30 in water (red). Error bars: standard deviations from \sim 8 hydrogels for each condition. (b,c) Example histograms of SMdM single-molecule displacements for RNase A (b) and IgG (c) under the two expansion conditions. Blue curves: MLE results, with the resultant 95% confidence intervals of D values marked in each plot.

For in-gel diffusion, SMdM indicated that in hydrogels expanded by 3.31 ± 0.30 in water (36× volume expansion; 0.24 wt% final polymer content), D of all diffusers remained largely unaffected, i.e., $D_{\text{gel}}/D_{\text{PBS}} \sim 1$ (Figure 2a). In contrast, in hydrogels expanded by 1.66 ± 0.14 in PBS (4.6× volume expansion; 1.9 wt% final polymer content), SMdM unveiled a striking size-

dependent suppression of diffusion (Figure 2a). Whereas the diffusivity of the 0.6 kDa Cy3B was only slightly impeded to 91±3% of its value in PBS, steady drops to 78±8%, 60±10%, and 50±10% of the PBS values were respectively found for the increasingly larger RNase A, BSA, and IgG. Examination of the SM*d*M-recorded transient single-molecule displacements yielded good fits to our random walk model (Figure 2bc), suggesting normal diffusion of the differently impeded proteins at the temporal (~500 μs) and length (~300 nm) scales of our experiments. This marked size-dependent depression of diffusion is consistent with a model in which as we reduce the mesh size of our hydrogel system to the few-nanometer scale,³⁷ larger molecules are more affected by the nanomatrix (schematics in Figure 1a).

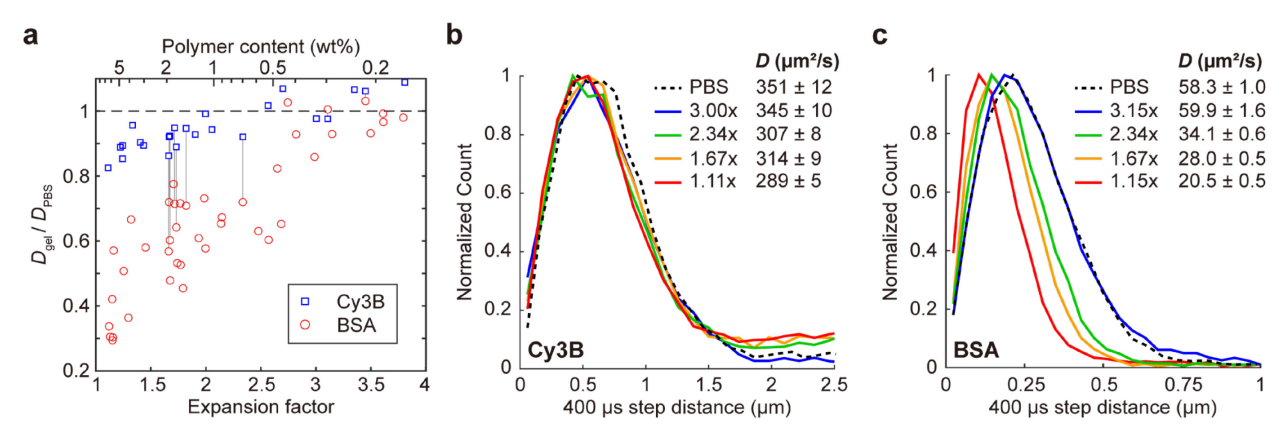


Figure 3. Contrasting diffusivity scaling behaviors in differently expanded hydrogels for a small dye and a protein. (a) The SMdM-determined in-gel diffusion coefficient *D* relative to that in the PBS buffer for the 0.6 kDa dye Cy3B (blue) and the 67 kDa protein BSA (red), in different hydrogel samples at varied expansion factors (bottom x-axis) and hence polymer contents (top x-axis). Vertical lines connect paired data, in which the diffusion of AF647-labeled BSA and Cy3B were sequentially measured through 2-color SMdM in the same gel sample. (b) Normalized count distributions of the SMdM-measured 400 μs single-molecule displacements for Cy3B diffusing in PBS (dash line) and in four hydrogel samples of different expansion factors (solid lines), with respective MLE results shown in the legend as 95% confidence intervals. (c) Similar to (b) but for the diffusion of BSA.

We next focused on Cy3B and BSA as representative small and macro- molecules, and fine-tuned the hydrogel expansion factor to examine how their diffusion transits from unimpeded to impeded as the meshwork size is gradually reduced. SMdM showed that for the 0.6 kDa small molecule Cy3B (Figure 3ab), only mild drops in D occurred when the linear expansion factor was reduced to <2 (8× volume expansion; 1.1 wt% polymer content), with the D value lowering to ~85% of that in PBS in the limit of expansion factors of 1.1-1.2 (~6 wt% polymer content). In

contrast, for the 67 kDa BSA protein (Figure 3ac), SMdM unveiled notable decreases in D for expansion factors <3 (27× volume expansion; 0.33 wt% polymer content), and D dropped to 50-70% and ~30% of that in PBS at expansion factors of ~2 (1.1 wt% polymer content) and 1.1-1.2 (~6 wt% polymer content), respectively.

To further substantiate the contrasting scaling behaviors of Cy3B and BSA, in several gel samples we examined the diffusion of both molecules by performing two-color SMdM, using the spectrally distinct Alexa Fluor 647 (AF647) to label BSA (Figure S4). The sequentially acquired SMdM data in the two color channels (connected by vertical lines in Figure 3a) thus confirmed in the same samples distinct relative D values over PBS, with the diffusion of BSA being substantially more suppressed. Together, these results indicate that the diffusion of the 67 kDa BSA molecule is progressively more impaired as the hydrogel mesh size is continuously reduced to reach polymer contents of >0.33 wt%, whereas the 0.6 kDa Cy3B does not quite "sense" the existence of the polymer nanomatrix even at much higher polymer contents.

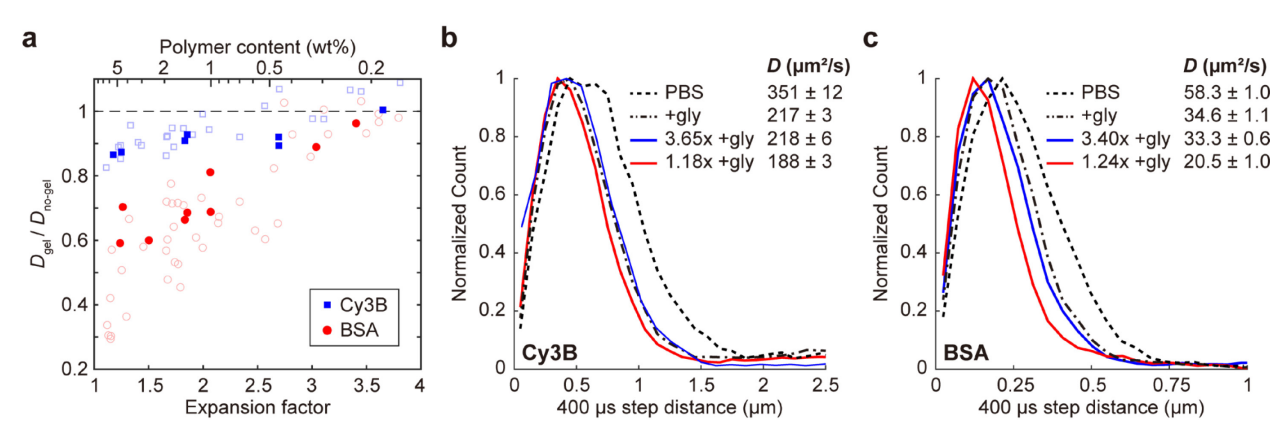


Figure 4. Uncoupled diffusion suppressions by the solution viscosity and by the hydrogel nanomatrix. (a) Solid symbols: the SMdM-determined in-gel diffusion coefficient *D* of Cy3B (blue) and BSA (red), in hydrogels expanded at different expansion factors (bottom x-axis) and hence polymer contents (top x-axis) in solutions containing 18 wt% glycerol, relative to that in the 18 wt% glycerol solution. Hollow symbols: reproduced from Figure 3a for in-gel *D* relative to no-gel for hydrogels expanded in PBS. (b) Normalized count distributions of the SMdM-measured 400 μs single-molecule displacements for Cy3B diffusing in PBS (dash line), in the 18 wt% glycerol solution (dash-dot line), and in two hydrogels of different expansion factors in 18 wt% glycerol solutions (solid lines). MLE results are shown as 95% confidence intervals in the legend. (c) Similar to (b) but for the diffusion of BSA.

As intracellular diffusion is suppressed by both the nanoscale architecture of the cell and the 20-40% higher viscosity of the cytosol over water, 12 we next probed, with our expandable

hydrogel system, whether the two effects would independently modulate the diffusion of small and macro- molecules. To this end, we thickened the solution by adding the inert small molecule glycerol. 38,39 SMdM showed that in an 18 wt% glycerol solution, the D values of Cy3B and BSA dropped to 217 and 35 μ m 2 /s (dash-dot curves in Figure 4bc), respectively, corresponding to 62% and 60% of that in PBS (dash curves in Figure 4bc). These diffuser size-insensitive values match that predicted (60%) through scaling the known glycerol concentration-dependent viscosity. 38,39

We next examined the diffusion of both molecules in our hydrogel system expanded in the presence of 18 wt% of glycerol. Interestingly, as we plotted the SMdM-determined relative D values over that in the 18 wt% glycerol solution, we observed similar expansion-factor-dependent D scaling as hydrogels expanded in PBS (Figure 4a). Thus, obstruction of diffusion due to the hydrogel nanomatrix is uncoupled from diffusion suppressions due to higher solution viscosities, and the two factors may each separately scale down the D values to produce the final diffusion slowdown.

Conclusion

Together, by repurposing the recently popularized expansion microscopy to achieve controlled tuning of the hydrogel meshwork size, we examined the in-gel diffusion of small and macro-molecules over a wide range of polymer fractions of ~0.14–7 wt%. Through SMdM single-molecule measurements, we thus showed that with a constant meshwork size, larger molecules exhibited more impeded diffusion, and that for the same molecule, diffusion is progressively more suppressed as the meshwork size was reduced, and this effect was more prominent for the larger molecules. Whereas similar trends have been reported with hydrogels prepared from discrete initial monomer concentrations, ^{18,19,40} our approach both ensured the geometric expansion of meshwork size as the only variable between different samples and achieved continuous fine-tuning of the meshwork size. Moreover, by thickening the solution while conserving the hydrogel expansion factors, we showed that the meshwork-induced obstruction of diffusion is uncoupled from the suppression of diffusion from increased solution viscosities.

In complex systems like the cell, the two mechanisms, respectively being diffuser-size dependent and independent, should separately scale down D to produce the final diffusion slowdown. On this discussion, our observation that the formal factor caused minimal slowdowns

for Cy3B, even in the limit of low expansion factors where substantial diffusion obstruction was observed for macromolecules, echoes our recent finding that the intracellular D of small molecules is only modestly depressed to ~70% of that in water by the slightly higher viscosity of the cytosol. Meanwhile, the demonstrated unconventional use of expandable hydrogel and expansion microscopy for physical-parameter tunning provides an appealing path toward the future development of manipulation and measurement tools.

ASSOCIATED CONTENT

The Supporting Information is available free of charge on the ACS Publications website.

Schematics of the sample-preparation workflow; tuning the hydrogel expansion factor through ionic strength; reference diffusivities in PBS; illustration of 2-color SMdM. (PDF)

AUTHOR INFORMATION

Corresponding Author

* xuk@berkeley.edu

Notes

The authors declare no competing financial interest.

ACKNOWLEDGMENT

We acknowledge support from the National Science Foundation (CHE-2203518), the Packard Fellowships for Science and Engineering, and the Heising-Simons Faculty Fellows award.

REFERENCES

- (1) Verkman, A. S. Solute and macromolecule diffusion in cellular aqueous compartments. *Trends Biochem. Sci.* **2002**, *27*, 27-33.
- (2) Soh, S.; Byrska, M.; Kandere-Grzybowska, K.; Grzybowski, B. A. Reaction-Diffusion Systems in Intracellular Molecular Transport and Control. *Angew. Chem.-Int. Edit.* **2010**, *49*, 4170-4198.
- (3) Shen, H.; Tauzin, L. J.; Baiyasi, R.; Wang, W. X.; Moringo, N.; Shuang, B.; Landes, C. F. Single particle tracking: from theory to biophysical applications. *Chem. Rev.* **2017**, *117*, 7331-7376.

- (4) Mogre, S. S.; Brown, A. I.; Koslover, E. F. Getting around the cell: physical transport in the intracellular world. *Phys. Biol.* **2020**, *17*, 061003.
- (5) Milo, R.; Phillips, R. Cell Biology by the Numbers; Garland Science: New York, NY, 2016.
- (6) Lukacs, G. L.; Haggie, P.; Seksek, O.; Lechardeur, D.; Freedman, N.; Verkman, A. S. Size-dependent DNA Mobility in Cytoplasm and Nucleus. *J. Biol. Chem.* **2000**, *275*, 1625-1629.
- (7) Dauty, E.; Verkman, A. S. Actin cytoskeleton as the principal determinant of size-dependent DNA mobility in cytoplasm. *J. Biol. Chem.* **2005**, *280*, 7823-7828.
- (8) Kumar, M.; Mommer, M. S.; Sourjik, V. Mobility of cytoplasmic, membrane, and DNA-binding proteins in *Escherichia coli. Biophys. J.* **2010**, *98*, 552-559.
- (9) Kalwarczyk, T.; Ziębacz, N.; Bielejewska, A.; Zaboklicka, E.; Koynov, K.; Szymański, J.; Wilk, A.; Patkowski, A.; Gapiński, J.; Butt, H.-J. *et al.* Comparative analysis of viscosity of complex liquids and cytoplasm of mammalian cells at the nanoscale. *Nano Lett.* **2011**, *11*, 2157-2163.
- (10) Śmigiel, W. M.; Mantovanelli, L.; Linnik, D. S.; Punter, M.; Silberberg, J.; Xiang, L.; Xu, K.; Poolman, B. Protein diffusion in Escherichia coli cytoplasm scales with the mass of the complexes and is location dependent. *Sci. Adv.* **2022**, *8*, eabo5387.
- (11) Choi, A. A.; Xiang, L.; Li, W.; Xu, K. Single-molecule displacement mapping indicates unhindered intracellular diffusion of small (~1 kDa) solutes. *bioRxiv* **2023**, 2023.01.26.525579.
- (12) Fushimi, K.; Verkman, A. S. Low Viscosity in the Aqueous Domain of Cell Cytoplasm Measured by Picosecond Polarization Microfluorimetry. *J. Cell Biol.* **1991**, *112*, 719-725.
- (13) Li, J.; Mooney, D. J. Designing hydrogels for controlled drug delivery. *Nat. Rev. Mater.* **2016**, *I*, 16071.
- (14) Saini, A.; Kisley, L. Fluorescence microscopy of biophysical protein dynamics in nanoporous hydrogels. *J. Appl. Phys.* **2019**, *126*, 081101.
- (15) Guo, Y.; Bae, J.; Fang, Z.; Li, P.; Zhao, F.; Yu, G. Hydrogels and Hydrogel-Derived Materials for Energy and Water Sustainability. *Chem. Rev.* **2020**, *120*, 7642-7707.
- (16) Yuk, H.; Wu, J.; Zhao, X. Hydrogel interfaces for merging humans and machines. *Nat. Rev. Mater.* **2022**, *7*, 935-952.
- (17) Kisley, L.; Brunetti, R.; Tauzin, L. J.; Shuang, B.; Yi, X.; Kirkeminde, A. W.; Higgins, D. A.; Weiss, S.; Landes, C. F. Characterization of Porous Materials by Fluorescence Correlation Spectroscopy Superresolution Optical Fluctuation Imaging. *ACS Nano* **2015**, *9*, 9158-9166.
- (18) Sandrin, D.; Wagner, D.; Sitta, C. E.; Thoma, R.; Felekyan, S.; Hermes, H. E.; Janiak, C.; de Sousa Amadeu, N.; Kühnemuth, R.; Löwen, H. *et al.* Diffusion of macromolecules in a polymer hydrogel: from microscopic to macroscopic scales. *Phys. Chem. Chem. Phys.* **2016**, *18*, 12860-12876.
- (19) Offeddu, G. S.; Axpe, E.; Harley, B. A. C.; Oyen, M. L. Relationship between permeability and diffusivity in polyethylene glycol hydrogels. *AIP Adv.* **2018**, *8*, 105006.
- (20) Kremer, M.; Pothmann, E.; Roessler, T.; Baker, J.; Yee, A.; Blanch, H.; Prausnitz, J. M. Pore-Size Distributions of Cationic Polyacrylamide Hydrogels Varying in Initial Monomer Concentration and Cross-Linker/Monomer Ratio. *Macromolecules* **1994**, *27*, 2965-2973.
- (21) Chen, F.; Tillberg, P. W.; Boyden, E. S. Expansion microscopy. Science 2015, 347, 543-548.
- (22) Wassie, A. T.; Zhao, Y.; Boyden, E. S. Expansion microscopy: principles and uses in biological research. *Nat. Methods* **2019**, *16*, 33-41.
- (23) Zwettler, F. U.; Reinhard, S.; Gambarotto, D.; Bell, T. D. M.; Hamel, V.; Guichard, P.; Sauer, M. Molecular resolution imaging by post-labeling expansion single-molecule localization microscopy (ExSMLM). *Nat. Commun.* **2020**, *11*, 3388.
- (24) Kang, M.; Lee, J.; Ko, S.; Shim, S.-H. Prelabeling Expansion Single-Molecule Localization Microscopy with Minimal Linkage Error. *ChemBioChem* **2021**, *22*, 1396-1399.

- (25) Lee, H.; Yu, C.-C.; Boyden, E. S.; Zhuang, X.; Kosuri, P. Tetra-gel enables superior accuracy in combined super-resolution imaging and expansion microscopy. *Sci. Rep.* **2021**, *11*, 16944.
- (26) Shi, X.; Li, Q.; Dai, Z.; Tran, A. A.; Feng, S.; Ramirez, A. D.; Lin, Z.; Wang, X.; Chow, T. T.; Chen, J. et al. Label-retention expansion microscopy. J. Cell Biol. 2021, 220, e202105067.
- (27) Xiang, L.; Chen, K.; Yan, R.; Li, W.; Xu, K. Single-molecule displacement mapping unveils nanoscale heterogeneities in intracellular diffusivity. *Nat. Methods* **2020**, *17*, 524-530.
- (28) Yan, R.; Chen, K.; Xu, K. Probing nanoscale diffusional heterogeneities in cellular membranes through multidimensional single-molecule and super-resolution microscopy. *J. Am. Chem. Soc.* **2020**, *142*, 18866-18873.
- (29) Choi, A. A.; Park, H. H.; Chen, K.; Yan, R.; Li, W.; Xu, K. Displacement statistics of unhindered single molecules show no enhanced diffusion in enzymatic reactions. *J. Am. Chem. Soc.* **2022**, *144*, 4839-4844.
- (30) Xie, X. S.; Yu, J.; Yang, W. Y. Living cells as test tubes. Science 2006, 312, 228-230.
- (31) Xie, X. S.; Choi, P. J.; Li, G. W.; Lee, N. K.; Lia, G. Single-molecule approach to molecular biology in living bacterial cells. *Ann. Rev. Biophys.* **2008**, *37*, 417-444.
- (32) Asano, S. M.; Gao, R.; Wassie, A. T.; Tillberg, P. W.; Chen, F.; Boyden, E. S. Expansion Microscopy: Protocols for Imaging Proteins and RNA in Cells and Tissues. *Curr. Protoc. Cell Biol.* **2018**, *80*, e56.
- (33) Truckenbrodt, S.; Sommer, C.; Rizzoli, S. O.; Danzl, J. G. A practical guide to optimization in X10 expansion microscopy. *Nat. Protoc.* **2019**, *14*, 832-863.
- (34) Tanaka, T.; Fillmore, D.; Sun, S.-T.; Nishio, I.; Swislow, G.; Shah, A. Phase Transitions in Ionic Gels. *Phys. Rev. Lett.* **1980**, *45*, 1636-1639.
- (35) Ohmine, I.; Tanaka, T. Salt effects on the phase transition of ionic gels. *J. Chem. Phys.* **1982**, 77, 5725-5729.
- (36) Young, M. E.; Carroad, P. A.; Bell, R. L. Estimation of diffusion coefficients of proteins. *Biotechnol. Bioeng.* **1980**, *22*, 947-955.
- (37) Cohen, Y.; Ramon, O.; Kopelman, I. J.; Mizrahi, S. Characterization of inhomogeneous polyacrylamide hydrogels. *J. Polym. Sci. B Polym. Phys.* **1992**, *30*, 1055-1067.
- (38) Sheely, M. L. Glycerol viscosity tables. Ind. Eng. Chem. 1932, 24, 1060-1064.
- (39) Wang, Q.; Moerner, W. E. Single-molecule motions enable direct visualization of biomolecular interactions in solution. *Nat. Methods* **2014**, *11*, 555-558.
- (40) Axpe, E.; Chan, D.; Offeddu, G. S.; Chang, Y.; Merida, D.; Hernandez, H. L.; Appel, E. A. A multiscale model for solute diffusion in hydrogels. *Macromolecules* **2019**, *52*, 6889-6897.

TOC Graphic

